Tapered labyrinthine acoustic metamaterials for broadband impedance matching

Yangbo Xie, Adam Konneker, Bogdan-Ioan Popa, and Steven A. Cummer[a)]
Department of Electrical and Computer Engineering, Duke University, Durham, North Carolina 27708, USA

(Received 14 September 2013; accepted 3 November 2013; published online 14 November 2013)

We present five kinds of labyrinthine or space-coiling acoustic metamaterials with tapered channels and apertures. These designs exhibit negative index behavior with modest dispersion, and also have substantially improved impedance matching compared to previously investigated labyrinthine cells. Experimentally measured effective material parameters are in good agreement with numerically computed results for the first two designs. Numerical results are presented for the other three unit cells. By virtue of their design tunability and small size, these tapered labyrinthine acoustic metamaterials show potential as building blocks for a wide range of acoustic wave manipulation and imaging applications. © *2013 AIP Publishing LLC*. [http://dx.doi.org/10.1063/1.4831770]

Acoustic metamaterials are engineered structures that feature unusual effective material parameters such as density, bulk modulus, and refractive index with negative,[1–3] close-to-zero,[4] or highly anisotropic[5,6] values. In the last decade of development of this area,[7] attention has been focused primarily on two types of unit cell design strategies: locally resonant materials, and effective medium theory based composites. Examples of the former are Helmholtz resonator based unit cells[3,8] and membrane-based ones.[2,9] References 6, 10–13 show examples of the effective medium theory based type. Recently, design of geometry-based non-locally resonant unit cells was theoretically proposed[14] and experimentally verified.[15–17] These kinds of unit cell can be designed to possess extreme parameters with low absorption and wide operating bandwidth. However, impedance matching is relatively poor in labyrinthine designs that have been reported so far.[14–17]

In this paper, we describe and analyze five examples of labyrinthine acoustic metamaterial unit cell designs with tapered structures and present their measured and/or simulated effective material parameters. All these designs exhibit modest dispersion in their negative refractive index bands and significantly improved impedance matching compared with the previously presented labyrinthine unit cells.[14–17] Besides their attractive refractive index and impedance, the geometry of these metamaterials can be easily tailored to obtain specific parameters and can be reliably fabricated with existing rapid prototyping technology. Possible applications based on these unit cells include transformation acoustic devices,[18] acoustic diffraction gratings, acoustic holography, and other coherent modulation system.

Tapered structures are common in electromagnetic antenna and transmission line designs for optimizing impedance matching and increasing operating bandwidth.[19] In applied acoustics, tapered acoustic waveguides are also widely utilized in musical instruments and loudspeaker systems for similar purposes.[20] The gradually varying cross section of a tapered structure, such as an exponential acoustic horn, diminishes the mismatch of the transverse components of a wave caused by the sudden change of cross sectional area,[21] thus, increasing the efficiency of power transmission. Similar design concepts can be applied to metamaterial unit cells to improve impedance matching and increase the bandwidth of the desired properties. Assuming we have a tapered structure whose cross-section area along the wave travelling path can be expressed as $S(\zeta)$, in which ζ is the spatial coordinate along this path, then using a long wavelength approximation, the acoustic wave equation can be expressed as $\frac{\partial^2 p}{\partial^2 \zeta} + \frac{\partial \ln S(\zeta)}{\partial \zeta}\frac{\partial p}{\partial \zeta} = \frac{1}{c^2}\frac{\partial^2 p}{\partial^2 t}$, known as Webster's equation.[22] The second term in this equation will lead to a geometry-dependent dispersion relation of the complex wave vector k. As a result, there will be a cutoff frequency ω_c and the complex impedance can be expressed[23] as $Z_0' = Z_0\sqrt{1-(\frac{\omega_c}{\omega})^2} + j\frac{\omega_c}{\omega}$, both of which are dependent on the parameter $S(\zeta)$. Therefore, by modifying the geometry of the wave-guiding structure of the unit cell we can tune the impedance for the purpose of better impedance matching.

We will present the unit cell designs and the experimentally and/or numerically retrieved material parameters as follows. All the fabricated samples shown in the paper are made of acrylonitrile butadiene styrene (ABS) thermoplastic and were fabricated via 3D printing using fused deposition modeling (FDM) technology. The effective parameter measurements were performed with our lab-made one dimensional waveguide[10] utilizing a reflection-transmission retrieval procedure.[24] Calculated material parameters were obtained using a commercial finite element analysis (FEA) solver COMSOL MULTIPHYSICS.

The first design is a variation to the previously investigated labyrinthine or space-coiling unit cell.[14,15] A photograph of a 3D printed sample is given in Fig. 1(a). This new unit cell shares similar coiling structure as the original design,[14,15] however, the inner meandering paths are rotated by an angle of about 30° to form horn-shaped ports. The port aperture is 6.9 mm, which is about 4.3 times the width of the inner meandering channel. Comparing the impedance of the horn-port labyrinthine cell with that of the original labyrinthine cell described in Ref. 1, we find that of the new unit

[a)]Electronic mail: cummer@ee.duke.edu

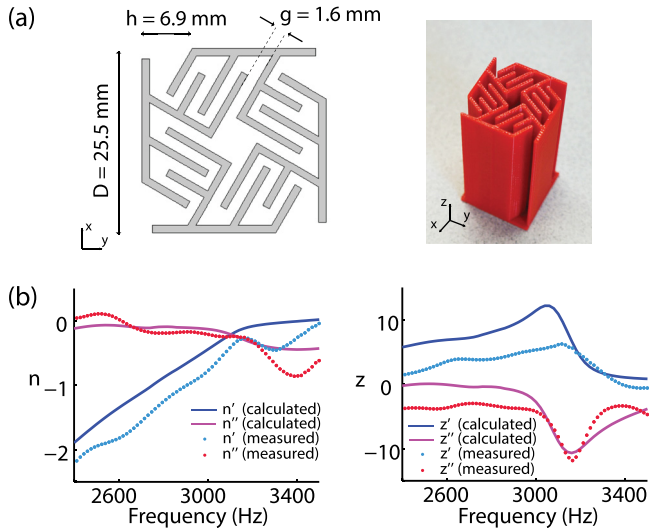

FIG. 1. Horn-port labyrinthine unit cell. (a) Cross sectional geometry and a photograph of a 3D printed sample. (b) Experimentally measured and calculated refractive index and impedance.

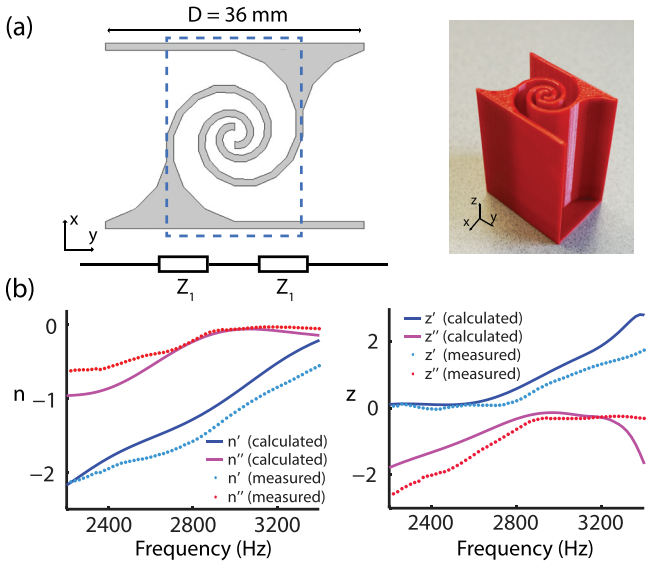

FIG. 2. Anisotropic spiral unit cell. (a) Geometry of the cross section of the unit cell, an equivalent transmission line diagram and a photograph of a 3D printed sample. (b) Experimentally measured and numerically retrieved refractive index and impedance.

cell is 30% less than that of the original design over the frequency range, where the impedance of both unit cells are away from resonance. Figure 1(c) compares the experimentally measured and numerically computed refractive index and impedance. The measured results match reasonably well with the FEA calculations and minor discrepancies are attributed to fabrication defects. Both measured and simulated results show negative refractive index ranging from 2400 Hz to 3000 Hz with imaginary parts close to zero. In the range of negative refractive index, the impedance remains relatively constant and a resonance peak occurs around the frequency when the refractive index is close to zero.

Second, we will present three unit cell designs which we have termed spiral labyrinthine unit cells, which are inspired by the spiral geometry of many gastropod shells. Spirals are favored both by nature and engineers and are a tapered structure with a simple mathematical description. Natural and man-made examples involving spiral geometry can be found in the cochlea of the inner ear, architectural designs, and microwave antennas.

Figure 2(a) is the cross section and a photograph of an anisotropic spiral unit cell which we designed and fabricated via 3D printing. This kind of unit cell will be utilized to modulate wave propagating along y axis. The spiral curve within the blue dashed rectangle in Figure 2(a) can be expressed in parametric form as $r(\theta) = a(\theta)e^{b(\theta)\times\theta}$ $(\theta_1 < \theta < \theta_2)$. The tapering structure outside the blue dashed rectangular region only slightly contributes to impedance matching and wave modulation. This part is designed as a reservoir space to accommodate higher level of coiling relative to the example presented in Figure 2(a) within the same unit cell side length.

By tuning the two angular dependent coefficients $a(\theta)$, $b(\theta)$ as well as angular span θ_1 and θ_2, a large range of attainable effective parameters can be achieved. For example, we have designed and tested a set of 1D spiral unit cells which can completely cover a full 2π difference of modulated phase angle with only two layers of unit cells.

We define here a geometric factor termed as coiling coefficient η. It describes the degree of space coiling of the unit cell: $\eta = L_{av}/D$, in which L_{av} is the average wave path inside the coiling channel of a unit cell and D is the unit cell side length along the wave propagation direction. For the anisotropic spiral unit cell, the coiling coefficient is about 3.1, meaning that the length of the meandering path inside the unit cell is 3.1 times the side length of the cell. A rough estimation of the refractive index of the unit cell can be formulated[16] as $n_{eff} \approx \eta - \frac{2\pi c}{\omega D}$.

The impedance $Z_{eff} = R_{eff} + jX_{eff}$ of the anisotropic spiral unit cell is dominated by imaginary part jX_{eff} below frequency 2700 Hz, thus, the transmission through the unit cell is relatively low since transmitted power $P_{tr} \propto R_{eff}$. This dispersion property is similar to an exponential horn waveguide characterized as $r(\beta) = ae^{h\beta}$, which is a high-pass structure whose cutoff frequency depends on its geometrical factor h. The high-pass property of the anisotropic unit cell is expected since its impedance can be regarded as a series connection of two identical quasi-exponential waveguides, as depicted in the equivalent distributed transmission line model in Figure 2(a). For applications requiring relatively high transmission, frequency from 2550 Hz through 3400 Hz where transmission surpasses 70% is likely to be attractive. Around 3000 Hz, the transmission reaches the peak value of 93%. It is worth noting that the uniqueness of the frequency span from 2550 Hz to 3400 Hz lies in the simultaneous occurrence of high transmission and negative refractive index (n varies from -1.9 at 2550 Hz to -0.56 at 3400 Hz).

The above anisotropic unit cell is designed for one-dimensional applications such as gratings or holographic modulating surface. An isotropic version of the spiral unit cell is illustrated in Figure 3(a). The coiling coefficient for this unit cell is estimated as $\eta \approx 3.95$ by taking the average path along the waveguiding channel inside the unit cell. The numerically retrieved parameters in Figure 3(b) show that the unit cell possesses a negative refractive index over the range from 2000 Hz to 3500 Hz. To analyse the dispersion of impedance of the isotropic unit cell, we simplify a unit cell as a distributed

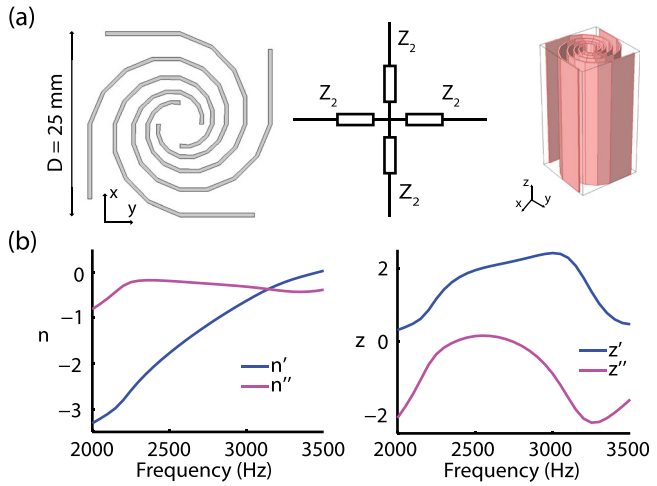

FIG. 3. Isotropic spiral unit cell. (a) Geometry of the cross section of the unit cell, an equivalent transmission line diagram and a computer generated 3D model. (b) Numerically retrieved refractive index and impedance.

transmission line as shown in Figure 3(a). Assuming the impedance of a single component is Z_2, then the ABCD matrix can be derived[19] as $\begin{bmatrix} A & B \\ C & D \end{bmatrix} = \begin{bmatrix} 3 & 4Z_2 \\ \frac{2}{Z_2} & 3 \end{bmatrix}$ and the complex transmission coefficient can be expressed as $S_{21}^{iso} = (3 + \frac{Z_0}{Z_2} + 2\frac{Z_2}{Z_0})^{-1}$. This will lead to a dispersion of transmission different from the above mentioned high-pass anisotropic spiral unit cell whose complex transmission can be expressed as $S_{21}^{aniso} = \frac{1}{1+Z_1}$. The transmission of the isotropic spiral cell ranges from 55% to 80% through the frequency span from 2000 Hz to 3500 Hz.

The proposed unit cell is made of aluminum assuming a density of 2700 kg/m^3 and a speed of sound of 6299 m/s. The designed thickness of the spiral geometry is 0.5 mm and the unit cell could be fabricated with existing high resolution Computer Numeric Control (CNC) machining systems. Besides the diffractive acoustics and coherent imaging applications as the anisotropic spiral unit cells, the isotropic version is likely to be useful in two dimensional transformation

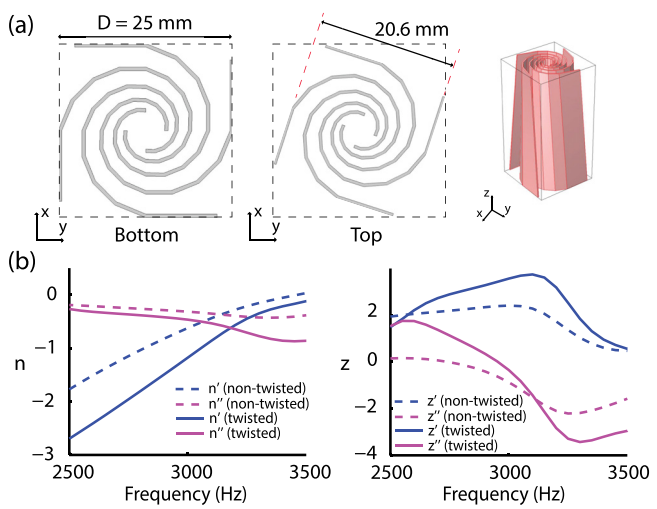

FIG. 4. Isotropic spiral unit cell with 18° twist along its height. (a) A computer generated 3D model. (b) Numerically retrieved refractive index and impedance.

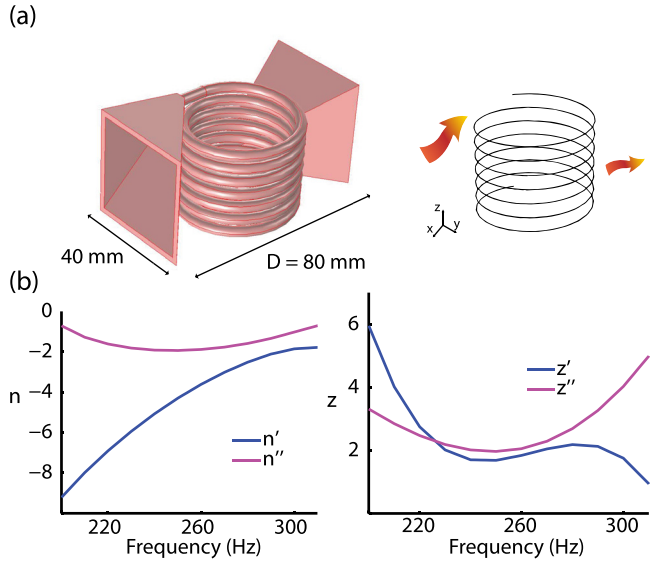

FIG. 5. Three-dimensional helical space-coiling unit cell (a) A computer generated 3D model and a schematic diagram of the propagation of acoustic wave inside the seven layer space coiling helical structure. (b) Numerically retrieved refractive index and impedance.

acoustics devices which need negative or high positive refractive index and low impedance.

If we twist the unit cell along its 5.08 cm height, additional degree of control over the dispersion can be achieved. A 3D model of the twisted cell is shown in Figure 4(a). This unit cell is derived from the non-twisted isotropic spiral unit cell described above. An angle of twist of 18° is applied along its height. In order to confine the rotated cross section within the 25 mm × 25 mm^2, the two-dimensional spiral geometry is gradually shrunk along the height. Figure 4(a) also compares the cross sections at the bottom and the top. The dimension of the top spiral geometry is 0.825 those of the bottom one and has a coiling coefficient of around 3.7. Therefore, the overall effective elapsed phase and the coiling coefficient of the unit cell are decreased comparing to the non-twisted version, confirmed by the numerically calculated parameters in Figure 4(b). The 18° twist shifts the dispersion of refractive index around 250 Hz in average towards higher frequency. Even higher degree of tunability of parameters can be achieved with larger twisted angles.

It is straightforward to extend the two-dimensional designs described above to three dimensions.[17] Figure 5 is an example of a three-dimensional version of the anisotropic spiral unit cell. The incident wave is guided by a tapered horn aperture to the central helical channel, where the transmission is close to unity, before it exits the unit cell through another tapered aperture. The exploitation of the third dimension significantly increases the level of space-coiling and lowers the interested negative refractive index frequency range. In the design presented in Figure 5, a high negative refractive index span can be found between 200 Hz and 300 Hz, where the transmission ranges from 35% to 50%. This example demonstrates the potential of applying three-dimensional labyrinthine cells for low frequency sound manipulation.[25]

In conclusion, we have demonstrated five labyrinthine or space-coiling acoustic metamaterial unit cell designs in

this paper. These designs employ tapered or spiral channels, which dramatically improves the impedance matching compared to the previously reported labyrinthine designs.[14–17] Numerically calculated results are shown and several are compared with experimentally retrieved parameters measured with 3D printed samples. These results confirm that broadband negative refractive index can be achieved with good impedance matching between the metamaterial unit cells and air. The ability to control phase and refractive index in this class of cell makes it potentially useful for transformation acoustic devices, acoustic diffraction gratings, acoustic holography, and acoustic imaging systems.

This work was supported by a Multidisciplinary University Research Initiative from the Office of Naval Research (Grant No. N00014-13-1-0631). We would also like to thank Patrick McGuire and Nikhil Bumb for their assistance with sample fabrication.

[1]J. Li and C. Chan, Phys. Rev. E **70**, 055602 (2004).
[2]Z. Yang, J. Mei, M. Yang, N. Chan, and P. Sheng, Phys. Rev. Lett. **101**, 204301 (2008).
[3]N. Fang, D. Xi, J. Xu, M. Ambati, W. Srituravanich, C. Sun, and X. Zhang, Nature Mater. **5**, 452 (2006).
[4]R. Fleury and A. Alù, Phys. Rev. Lett. **111**, 055501 (2013).
[5]J. Christensen and F. J. G. de Abajo, Phys. Rev. Lett. **108**, 124301 (2012).
[6]J. Li, L. Fok, X. Yin, G. Bartal, and X. Zhang, Nature Mater. **8**, 931 (2009).
[7]Z. Liu, X. Zhang, Y. Mao, Y. Zhu, Z. Yang, C. Chan, and P. Sheng, Science **289**, 1734 (2000).
[8]S. Zhang, L. Yin, and N. Fang, Phys. Rev. Lett. **102**, 194301 (2009).
[9]S. H. Lee, C. M. Park, Y. M. Seo, Z. G. Wang, and C. K. Kim, Phys. Rev. Lett. **104**, 054301 (2010).
[10]L. Zigoneanu, B.-I. Popa, A. F. Starr, and S. A. Cummer, J. Appl. Phys. **109**, 054906 (2011).
[11]B.-I. Popa, L. Zigoneanu, and S. A. Cummer, Phys. Rev. Lett. **106**, 253901 (2011).
[12]M. Farhat, S. Enoch, S. Guenneau, and A. Movchan, Phys. Rev. Lett. **101**, 134501 (2008).
[13]D. Torrent and J. Sánchez-Dehesa, New J. Phys. **10**, 023004 (2008).
[14]Z. Liang and J. Li, Phys. Rev. Lett. **108**, 114301 (2012).
[15]Y. Xie, B.-I. Popa, L. Zigoneanu, and S. A. Cummer, Phys. Rev. Lett. **110**, 175501 (2013).
[16]Z. Liang, T. Feng, S. Lok, F. Liu, K. B. Ng, C. H. Chan, J. Wang, S. Han, S. Lee, and J. Li, Sci. Rep. **3**, 1614 (2013).
[17]T. Frenzel, J. David Brehm, T. Buckmann, R. Schittny, M. Kadic, and M. Wegener, Appl. Phys. Lett. **103**, 061907 (2013).
[18]R. V. Craster and S. Guenneau, *Acoustic Metamaterials: Negative Refraction, Imaging, Lensing, and Cloaking* (Springer-Verlag, New York, 2013).
[19]D. M. Pozar, *Microwave Engineering* (Wiley, New York, 2009).
[20]N. N. H. Fletcher and T. D. Rossing, *The Physics of Musical Instruments* (Springer-Verlag, New York, 1998).
[21]D. T. Blackstock, *Fundamentals of Physical Acoustics* (Wiley, New York, 2000).
[22]A. G. Webster, Proc. Natl. Acad. Sci. USA **5**, 275 (1919).
[23]H. Kuttruff, *Acoustics: An Introduction* (Taylor & Francis, London, 2007).
[24]V. Fokin, M. Ambati, C. Sun, and X. Zhang, Phys. Rev. B **76**, 144302 (2007).
[25]J. Mei, G. Ma, M. Yang, Z. Yang, W. Wen, and P. Sheng, Nature Commun. **3**, 756 (2012).